Chinese Journal of
POLYMER SCIENCE

RESEARCH ARTICLE

https://doi.org/10.1007/s10118-026-3784-5
Chinese J. Polym. Sci.

Host-Guest Multiple Resonance Thermally Activated Delayed Fluorescent Copolymer Scintillators for X-ray Imaging

Kai Feng[a,†], Zong-Ji Ye[a,†], Wei-Guang Wang[a], Jia-Ni Huang[a], Xin Yan[a], Heng-Yu Cao[a], Zhi-Sheng Gao[a], Shu-Man Zhang[a], Si-Ming Chen[a], Huan-Huan Li[a*], and Ye Tao[a,b*]

[a] *State Key Laboratory of Flexible Electronics (LoFE) & Institute of Advanced Materials (IAM), Nanjing University of Posts & Telecommunications, Nanjing 210023, China*
[b] *State Key Laboratory of Coordination Chemistry, Nanjing University, Nanjing 210023, China*

Electronic Supplementary Information

Abstract Polymer-based scintillating materials hold considerable promise for a broad range of applications. However, their development has been constrained primarily by the intrinsically low exciton harvesting efficiency. Herein, we harness a host-guest energy transfer strategy to overcome this limitation. Through a simple radical polymerization, thermally activated delayed fluorescence units bearing a C=O/N resonance structure are embedded into a pyridine-containing copolymer framework. Using pyridine groups with high triplet energies as the host matrix effectively suppresses aggregation-caused quenching and maintains efficient reverse intersystem crossing process of luminescent thermally activated delayed fluorescence unit for high exciton harvesting. The resulting material exhibits intense photoluminescence and radioluminescence emission at 492 nm. Line-pair and modulation transfer function analyses further validate that the scintillator delivers a spatial resolution of 13.3 lp/mm and a detection limit of 390 nGy/s. X-ray imaging experiments demonstrate that the material can clearly resolve complex internal structures of diverse specimens, confirming its potential for industrial non-destructive testing. This work presents a flexible, high-resolution organic scintillator and paves the way for its deployment in multi-scenario X-ray imaging.

Keywords Polymer-based scintillating materials; Host-guest energy transfer strategy; Spatial resolution; Detection limit

Citation: Feng, K.; Ye, Z. J.; Wang, W. G.; Huang, J. N.; Yan, X.; Cao, H. Y.; Gao, Z. S.; Zhang, S. M.; Chen, S. M.; Li, H. H.; Tao, Y. Host-guest multiple resonance thermally activated delayed fluorescent copolymer scintillators for X-ray imaging. *Chinese J. Polym. Sci*. https://doi.org/10.1007/s10118-026-3784-5

INTRODUCTION

Scintillators are functional materials that absorb high-energy ionizing radiation and emit visible or ultraviolet photons.[1] These materials serve as core components in diverse applications, including medical X-ray diagnostics, industrial non-destructive testing, and radiation detection systems.[2–11] From a compositional perspective, typical scintillator materials are divided into two types: inorganic materials and organic molecules.[12,13] Organic scintillators offer the following merits: Their synthetic procedures are comparatively simple and inexpensive, and their molecular structures can be easily modified to satisfy the desired requirements. Remarkable progress has been made in the development of organic scintillator materials across diverse morphological categories, including single-crystalline solids, liquid solutions, and polymeric matrices.[3,14–17] The scintillation response of these materials is governed by fundamental radiation-matter interaction cascades, whereby high-energy photons interact with the bulk material through photoelectric absorption and Compton scattering to generate primary energetic electrons. These high-energy primary electrons subsequently undergo successive inelastic collisions with the surrounding atoms, producing copious secondary electrons alongside abundant electron-hole pairs through ionization and excitation events. According to the well-established spin statistics rule, the recombination of these charge carriers yields singlet and triplet excitonic states in an approximate 1:3 population ratio, where only the singlet fraction contributes to prompt radiative emission in conventional fluorescent systems, while the majority triplet fraction is typically dissipated *via* non-radiative pathways due to spin-forbidden transitions, inherently restricting exciton utilization efficiency.[18–23]

Recent exciton management strategies, including room-temperature phosphorescence materials, hybrid local and charge-transfer systems, open-shell organic radical scintillators, and thermally activated delayed fluorescence (TADF) materials, have substantially improved the exciton harvesting capacity, driving the iterative development of high-per-

* Corresponding authors, E-mail: iamhhli@njupt.edu.cn (H.H.L.)
E-mail: iamytao@njupt.edu.cn (Y.T)
† These authors contributed equally to this work.
Received May 20, 2026; Accepted June 14, 2026; Published online August 19, 2026

formance organic scintillators.[23–33] Among these platforms, multiple resonance TADF (MR-TADF) systems have attracted considerable attention. Their donor-acceptor molecular skeletons with orderly arranged electron-donating and electron-withdrawing units induce a complementary mesomeric resonance effect that effectively delocalizes frontier orbitals, thereby narrowing the singlet-triplet energy gap (ΔE_{ST}) to facilitate reverse intersystem crossing (RISC)-mediated triplet-to-singlet upconversion. Theoretically, this mechanism enables near-100% internal exciton utilization, overcoming the intrinsic 25% efficiency limit of traditional fluorescent scintillators. Complementarily, the rigid framework of the constrained aromatic core restricts intramolecular vibrational relaxation and structural distortion, generating an emission profile with a narrow full width at half maximum (FWHM) and high luminescence efficiency.

In this study, we developed a covalent host-guest sensitization strategy that harnesses TADF mechanisms to boost exciton utilization efficiency (Fig. 1a).[34–37] The MR-TADF emitters leverage the RISC mechanism to achieve near-100% exciton harvesting while embedding these chromophores into a tailored polymer matrix that isolates emissive units to suppress aggregation-caused quenching (ACQ). For the host-guest copolymer design, we incorporated pyridine moieties with high triplet energy levels into the backbone and chromophore of 7-(4-vinylphenyl)quinolino[3,2,1-de]acridine-5,9-dione (**VQA**) as MR-TADF units. The matched energy levels between the pyridine-based host and MR-TADF guest states facilitate efficient energy transfer (ET) to boost exciton harvesting. Leveraging an efficient host-guest ET, RL centered at 492 nm is realized, yielding a limit of detection (LOD) as low as 390 nGy/s. Furthermore, quantitative evaluation using the slanted-edge technique confirmed a spatial resolution of 13.3 lp/mm, enabling high-fidelity X-ray imaging. This work demonstrates a flexible, high-performance scintillator using a rational host-guest ET strategy, offering a promising platform for efficient X-ray detection.

EXPERIMENTAL

All experimental details and relevant synthesis characterizations are included in the electronic supplementary information (ESI).

RESULTS AND DISCUSSION

Synthesis

To validate the feasibility of the proposed covalent host-guest strategy, we implemented a facile free-radical copolymerization protocol using the MR-TADF chromophore **VQA** and 4-vinylpyridine (**4VP**) as comonomers, with 2,2'-azobis(2-methyl-

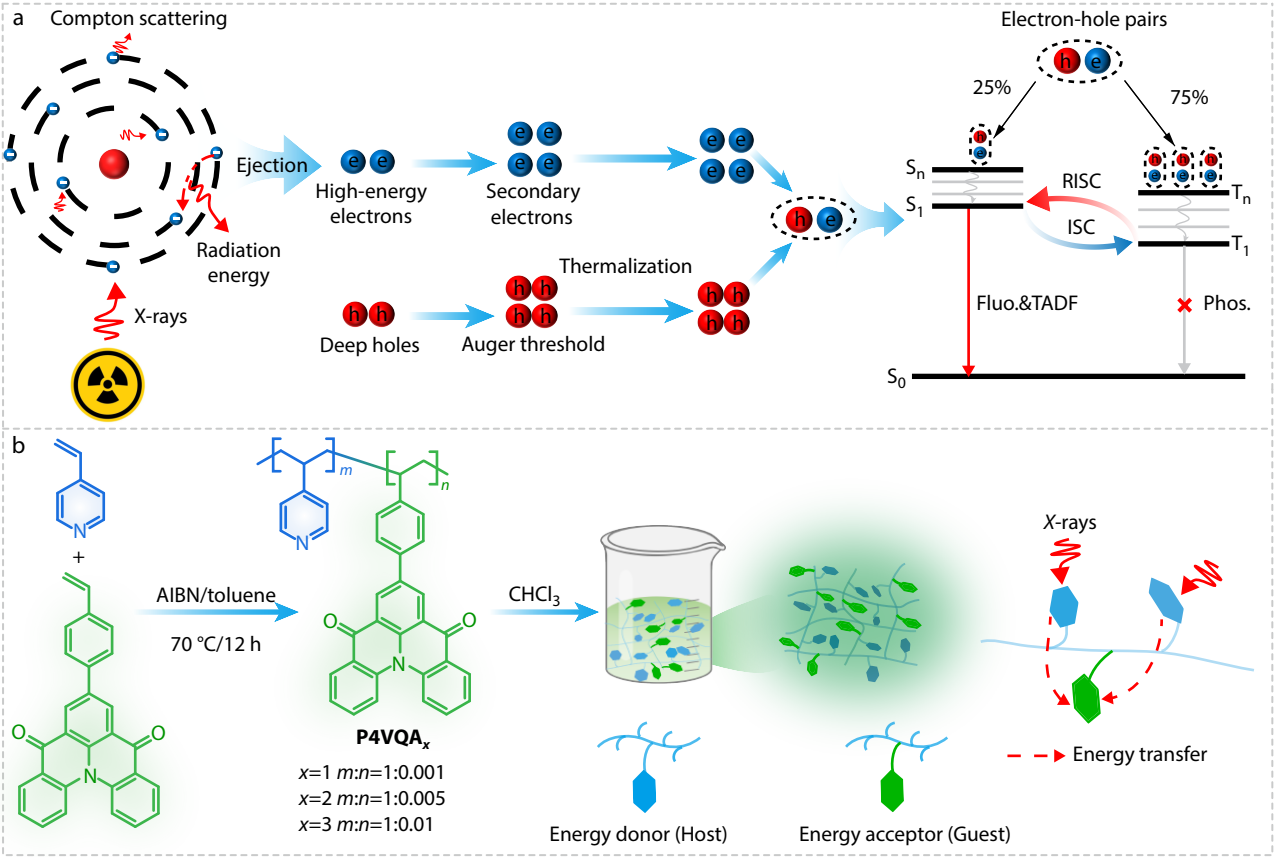

Fig. 1 Design strategy and mechanism of polymer scintillator. (a) Schematic illustration of the X-ray-to-light conversion cascade in organic scintillators and the radioluminescence (RL) mechanism of TADF scintillators; (b) Design route and molecular structure of copolymer and energy transfer pathway. ISC, intersystem crossing; RISC, reverse intersystem crossing; Fluo., fluorescence; Phos., phosphorescence; TADF, thermally activated delayed fluorescence; AIBN, azobisisobutyronitrile.

https://doi.org/10.1007/s10118-026-3784-5

propionitrile) serving as the thermal radical initiator (Figs. S1 and S2; Table S1 in ESI).[38] By systematically tuning the **4VP** to **VQA** (1000:1, 200:1, and 100:1), we synthesized a series of **P4VQA$_x$** copolymers (Fig. 1b). The amorphous nature of the resulting copolymers was confirmed by nuclear magnetic resonance spectroscopy, Fourier transform infrared spectroscopy, gel permeation chromatography, and powder X-ray diffraction, collectively verifying the successful incorporation of **VQA** chromophores into the **4VP**-based polymer backbone without disrupting the amorphous matrix structure (Figs. S3–S7 in ESI).

Radioluminescence Properties

To evaluate the potential of the designed polymers for scintillation applications, their RL properties were characterized under X-ray irradiation at 50 kV and 80 μA. The absorption spectra of **P4VP** and **P4VQA$_x$** were nearly identical (Fig. S8 in ESI), which confirms that the X-ray absorption originates primarily from the **4VP** units in the copolymer. Compared with **P4VQA$_1$**, the higher **VQA** doping levels in **P4VQA$_2$** and **P4VQA$_3$** promote the more efficient utilization of radiation-generated triplet excitons, leading to enhanced RL performance. Nevertheless, excessive **VQA** incorporation results in ACQ, which diminishes the RL intensity. Therefore, **P4VQA$_2$**, with its optimized guest concentration, exhibited the best RL properties (Fig. 2a). Under identical X-ray excitation conditions, **P4VQA$_2$** copolymer gives an estimated light yield of about 17368 photons MeV^{-1}, compared with 15900 photons MeV^{-1} for the commercial scintillator anthracene (Fig. S9 and Table S2 in ESI). The RL intensity of the copolymer **P4VQA$_2$** film was significantly higher than that of the film obtained by simply doping **VQA** into the **P4VP** matrix with VQA at the same concentration (Fig. S10 in ESI), highlighting the advantages of the copolymerization approach. To simulate practical X-ray detector configurations, we fabricated composite films by embedding the **P4VQA$_2$** polymer in a polysulfone (PSF) matrix for luminescence behavior investigation (Fig. 2b and Fig. S11 in ESI). PSF was incorporated as the host matrix to further enhance the flexibility and optical transparency of the scintillation film.

The RL output of the composite films exhibited a positive correlation with the **P4VQA$_2$** doping ratio, peaking at a loading concentration of 40 wt%, which was adopted for all subsequent scintillation performance evaluations and X-ray imaging experiments. As the X-ray dose rate increased, the RL intensities of the films increased proportionally (Fig. 2c). Further quantitative analysis established a robust linear dose-response relationship between **P4VQA$_2$** RL intensity and incident radiation dose rate, yielding a calculated LOD of 390 nGy/s (Fig. 2d).[39,40] This value is substantially below the 5.5 μGy/s threshold mandated for standard medical X-ray imaging procedures, confirming the suitability of the material for low-dose diagnostic applications.[41,42] To minimize photon loss during signal acquisition, the spectral compatibility between the photodetector sensitivity range and the scintillator emission profile is critical. As illustrated in Fig. 2(e), the emission profile of **P4VQA$_2$** exhibited excellent spectral compatibility with silicon photomultiplier detectors, effectively minimizing photon collection losses during signal acquisition. Furthermore, **P4VQA$_2$** demonstrated remarkable long-term stability under continuous X-ray irradiation for 3600 s and 210

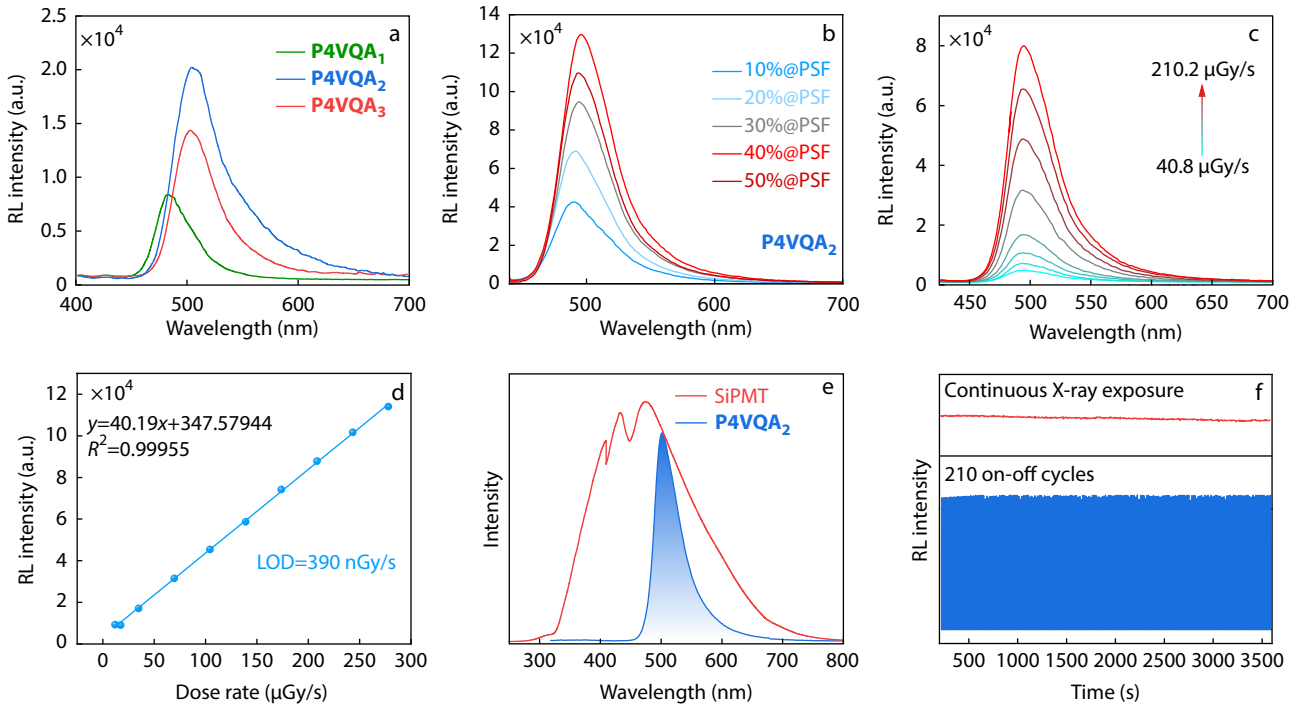

Fig. 2 RL characteristics of the MR-TADF copolymers under ambient conditions. (a) RL spectra of **P4VQA$_x$** scintillators; (b) RL spectra of **P4VQA$_2$** incorporated PSF film with different doping concentrations; (c) RL spectra and (d) corresponding RL intensities of 40 wt% **P4VQA$_2$** doped PSF film exposed to different radiation dose rates from 40.8 μGy/s to 210.2 μGy/s; (e) The spectral response curve of the silicon photomultiplier and RL spectrum of the 40 wt% **P4VQA$_2$** doped PSF film; (f) RL intensity stabilities under continuous X-ray exposure for 3600 s and under 210 repeated on-off irradiation cycles at a dose rate of 210.2 μGy/s.

https://doi.org/10.1007/s10118-026-3784-5

on/off cycles (Fig. 2f). The RL output maintains about 95% of its initial intensity across the full testing duration, confirming exceptional radiation hardness and robust operational stability under sustained high-dose excitation.[2,3,43]

Photophysical Properties

To further elucidate the structure-property relationships, we first performed absorption and steady-state photoluminescence (SSPL) spectral characterization of the **P4VQA$_x$** copolymers. A key observation is the exceptionally narrow emission bandwidth, which minimizes spectral overlap between the absorption and emission bands, effectively mitigating the severe self-absorption effects that commonly plague conventional organic scintillators (Fig. 3a).[3] Subsequent time-resolved fluorescence decay analysis revealed that the delayed fluorescence lifetimes of the polymer scintillators fell within the microsecond range (Fig. 3b), whereas the prompt fluorescence components exhibited nanosecond-scale lifetimes (Fig. S12 in ESI).[44,45] This structure effectively suppresses non-radiative vibrational relaxation, thereby preserving its intrinsic radiative decay characteristics and resulting in a similar lifetime in **P4VQA$_x$** copolymers. This distinct dual-lifetime behavior is characteristic of MR-TADF systems, confirming the successful integration of the TADF functionality into the polymer matrix. As shown in Fig. S13 (in ESI), the fluorescence peak was 492 nm, and the phosphorescence peak was 520 nm, thus yielding a ΔE_{ST} of approximately 0.14 eV. To further validate the MR-TADF mechanism, we recorded temperature-dependent SSPL spectra under 330 nm excitation over a 78–298 K range. As the temperature decreased, the prompt fluorescence intensity of **P4VQA$_2$** gradually diminished, accompanied by the appearance of a distinct new emission band centered at 520 nm (Fig. 3c). This low-temperature phosphorescence emission stems from suppression of the thermally activated RISC pathway, a characteristic signature of TADF systems.[46] The MR-TADF polymer with reduced ΔE_{ST} facilitates efficient RISC, which enables full harvesting of triplet excitons and significantly enhances photoluminescence quantum yield (PLQY). Notably, when the doping concentration of **VQA** increased, a slight decrease in the PLQY from 37.8% (**P4VQA$_2$**) to 34.5% (**P4VQA$_3$**) was observed (Fig. 3d), accompanied by a gradual broadening of the FWHM from 41 nm to 46 nm, along with a red-shift of the emission spectrum (Fig. S14 in ESI).

Furthermore, the pronounced spectral congruence between the SSPL profile of the **P4VP** homopolymer and the absorption band of **P4VQA$_2$** (Fig. 3e), coupled with the higher triplet energy level of **4VP** established the requisite photophysical foundation for ET from the **4VP** host to the **VQA** guest emitter (Fig. S15 in ESI). To elucidate the underlying luminescence mechanism, time-dependent density functional theory (TD-DFT) calculations.[47,48] The computed energy levels were as follows: S_1 (3.015 eV), T_1 (2.440 eV), T_2 (2.962 eV), T_3 (2.965 eV), T_4 (3.102 eV), and T_5 (3.185 eV). The large energy gap (0.575 eV) between S_1 and T_1 coupled with the minimal ΔE_{ST} between S_1 and T_2–T_5 indicates that ISC predominantly occurs between the S_1 and T_2–T_5 states, enabling efficient triplet-to-singlet upconversion (Fig. 3f). A plausible RL mechanism was proposed through combined RL and photophysical investigations. When X-rays interact with a copolymer, high-energy primary electrons are generated *via* photoelectric absorption and Compton scattering processes. These energetic electrons dissipate energy through successive in-

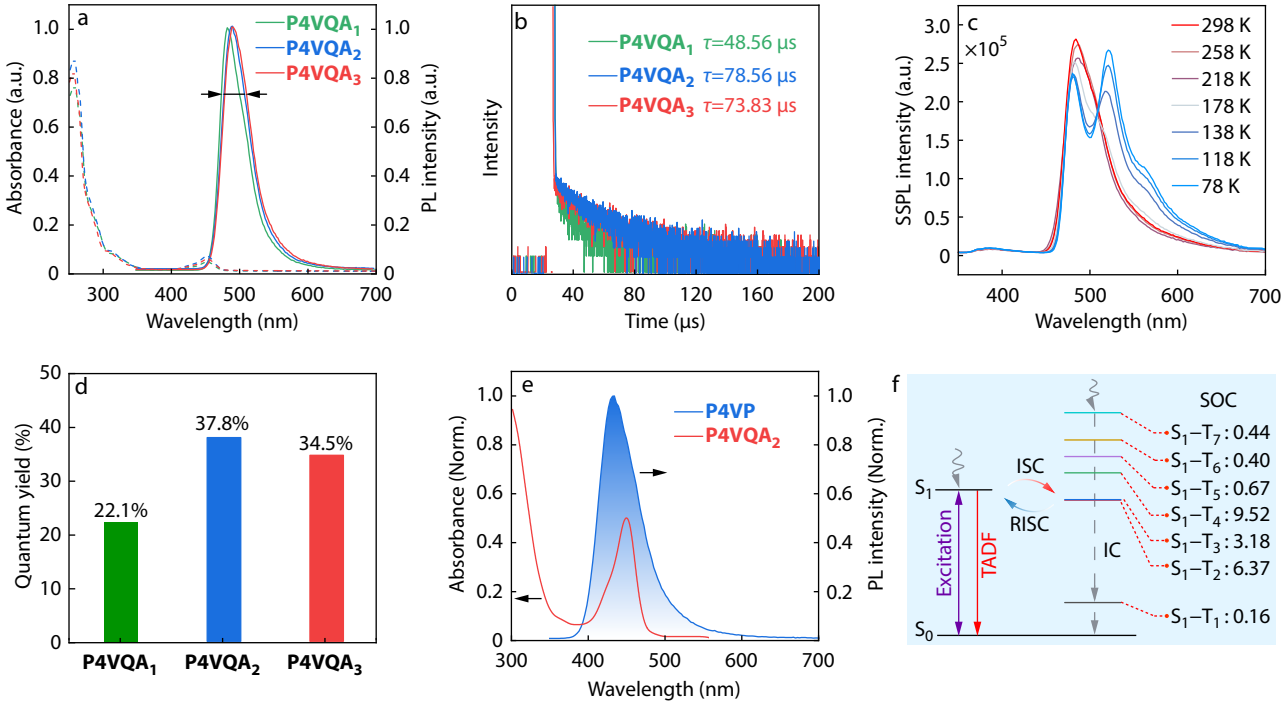

Fig. 3 Photophysical properties of MR-TADF copolymer scintillators. (a) Normalized absorption and emission spectra; (b) Delayed fluorescence lifetime decay profiles; (c) Temperature-dependent steady-state photoluminescence (SSPL) spectra of **P4VQA$_2$** ranging from 78 K to 298 K; (d) Photoluminescent quantum yields under 330 nm excitation; (e) SSPL spectrum of **P4VP** and absorbance spectrum of **P4VQA$_2$**; (f) Theoretically calculated excited energy levels and corresponding spin orbital coupling constants of **P4VQA**. The calculated mode is shown in ESI.

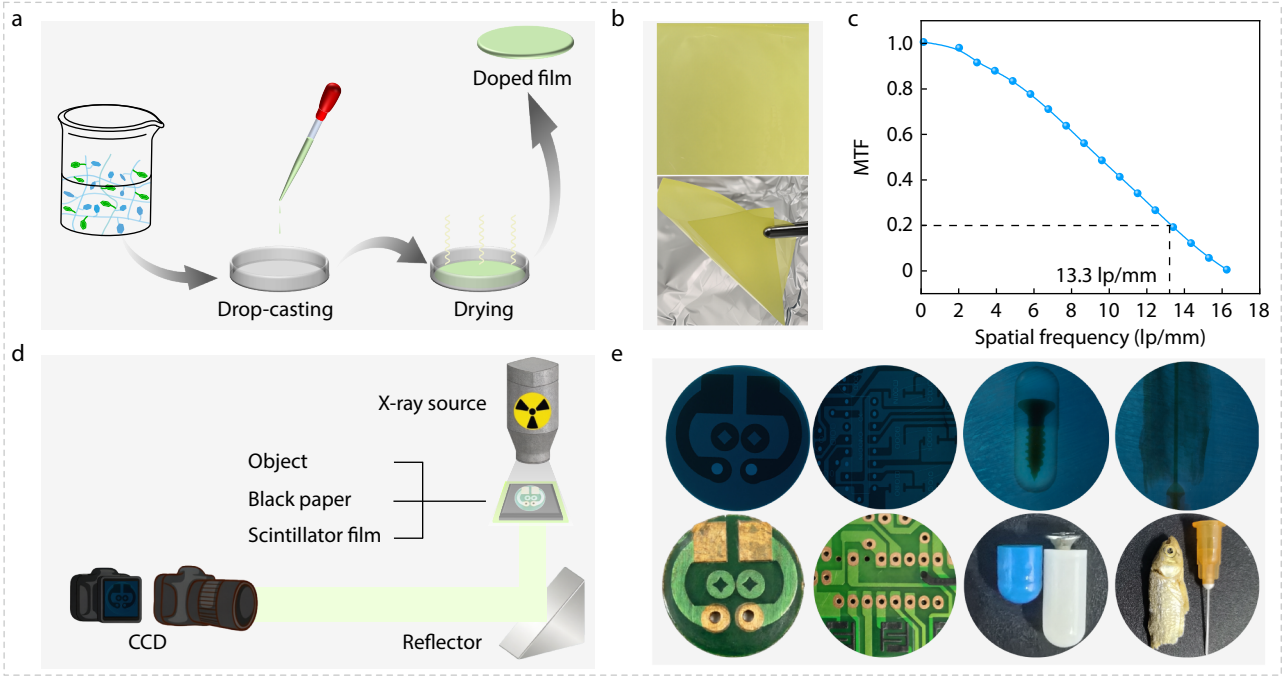

Fig. 4 Scintillation application of **P4VQA$_2$** doped PSF film. (a, b) Preparation procedures (a) and photographs (b) of **P4VQA$_2$** doped PSF film; (c) Modulation transfer function curves corresponding to the X-ray images obtained from the scintillation screen; (d) Schematic diagram of X-ray imaging equipment; (e) X-ray images of the cartoon image, electronic chip, capsule, and fish belly.

elastic collisions with the surrounding atoms, producing copious secondary electron cascades and electron-hole pairs. Charge carrier recombination subsequently generates singlet and triplet excitons at a theoretical 1:3 population ratio. With the aid of the RISC pathway, efficient triplet-to-singlet upconversion was achieved, substantially boosting the overall scintillation performance.

Application of Polymer Scintillator

By leveraging the exceptional X-ray sensitivity of the synthesized copolymers, we evaluated their potential for radiographic imaging applications. The superior scintillation performance of the **P4VQA$_2$** doped PSF film (Fig. 4a). As shown in Figs. 4(b) and Fig. S16 (in ESI), the prepared scintillator film has a thickness of only 0.05 mm, exhibiting high optical transparency and excellent bendability for X-ray imaging scenarios. Under X-ray excitation, the pure PSF films exhibited negligible RL. However, when doped with **P4VQA$_2$**, the same films produced bright scintillation. Therefore, the emission is almost entirely from **P4VQA$_2$**, and the PSF plays little role in the improved X-ray performance (Fig. S17 in ESI). The imaging performance of the material was quantitatively evaluated using the standard X-ray slanted-edge technique. Modulation transfer function measurements demonstrate that the screen can resolve fine structural details, achieving a spatial resolution of up to 13.3 lp/mm at an MTF value of 0.2 (Fig. 4c).

To further validate its practical utility, a custom-designed X-ray imaging platform was employed under meticulously optimized optical configurations (Fig. 4d). In this setup, the test object was strategically positioned in the beam path between the X-ray source and the scintillator panel. The polymeric scintillation screen successfully rendered the internal architectures of diverse specimens, ranging from intricate cartoon patterns and electronic chips to encapsulated screws and syringe needles embedded within fish tissue, thereby highlighting the exceptional imaging fidelity of this flexible scintillator film (Fig. 4e). Collectively, these results underscore the substantial potential of the polymer scintillator for advanced non-destructive testing, establishing a robust platform for high-performance, flexible X-ray imaging in demanding scenarios such as medical diagnostics, wearable radiation sensors, and curved-geometry tomography.

CONCLUSIONS

In summary, we successfully produced a copolymer containing the MR-TADF guest and host using a simple radical copolymerization method. The developed copolymers exhibited narrowband emissions at approximately 492 nm and PLQYs of approximately 38%. When irradiated by the X-ray radiation, the **P4VQA$_x$** shows good RL features, showing a good irradiation stability, high spatial resolution of 13.3 lp/mm and low detection limit of 390 nGy/s. This work utilized radical polymerization to fabricate a flexible, high-resolution organic scintillator, offering a versatile material platform for advanced X-ray imaging technologies.

Conflict of Interests

The authors declare no interest conflict.

Electronic Supplementary Information

Electronic supplementary information (ESI) is available free of

https://doi.org/10.1007/s10118-026-3784-5

charge in the online version of this article at http://doi.org/10.1007/s10118-026-3784-5.

Data Availability Statement

The data supporting the findings of this study are available from the corresponding author upon reasonable request.

ACKNOWLEDGMENTS

This study was financially supported in part by the National Natural Science Foundation of China (Nos. 22322106 and 62288102), the Basic Research Program of Jiangsu (No. BK20243057), the U35 Strong Foundation Program of Nanjing, and the Hua Li Talents Program of Nanjing University of Posts and Telecommunications.

REFERENCES

1 Xiao, S. B.; Zhang, X. Z.; Mao, X. C.; Yang, H. J.; Chen, Z. N.; Xu, L. J. Ultrahigh X-ray imaging spatial resolution enabled by an 0D Mn(II) hybrid scintillator. *Adv. Funct. Mater.* **2024**, *34*, 2404003.
2 Yuan, J. W.; Peng, Q. C.; Fu, J. C.; Yang, Q.; Gao, Z. Y.; Wang, Z. Y.; Li, K.; Zang, S. Q.; Tang, B. Z. Highly efficient stable luminescent radical-based X-ray scintillator. *J. Am. Chem. Soc.* **2023**, *145*, 27095−27102.
3 Li, H. H.; Liu, Y. T.; Zhao, W.; Cao, H. Y.; Yan, X.; Zhang, S. M.; Yan, X.; Li, H.; Tao, Y.; Xie, G. Z.; Li, W.; Chen, R. F.; Huang, W. Constructing organic phosphorescent scintillators with enhanced triplet exciton utilization through multi-mode radioluminescence for efficient X-ray imaging. *Adv. Mater.* **2024**, *36*, 2409338.
4 Wang, C.; Volotskova, O.; Lu, K. D.; Ahmad, M.; Sun, C.; Xing, L.; Lin, W. B. Synergistic assembly of heavy metal clusters and luminescent organic bridging ligands in metal-organic frameworks for highly efficient X-ray scintillation. *J. Am. Chem. Soc.* **2014**, *136*, 6171−6174.
5 Wang, Y.; Yu, J. H.; Zhou, Z. X.; Zhao, W. J.; Wang, Y. L.; Zhao, J. Q.; Ma, C. G.; Lin, Z. Y.; Wu, Y. Z.; Wang, X.; Ma, H. L.; Zhu, W. H. Organic ionic host-guest phosphor with dual-confined nonradiation for constructing ultrahigh-temperature X-ray scintillator. *J. Am. Chem. Soc.* **2025**, *147*, 11098−11107.
6 Morad, V.; Shynkarenko, Y.; Yakunin, S.; Brumberg, A.; Schaller, R. D.; Kovalenko, M. V. Disphenoidal zero-dimensional lead, tin, and germanium halides: highly emissive singlet and triplet self-trapped excitons and X-ray scintillation. *J. Am. Chem. Soc.* **2019**, *141*, 9764−9768.
7 Gandini, M.; Villa, I.; Beretta, M.; Gotti, C.; Imran, M.; Carulli, F.; Fantuzzi, E.; Sassi, M.; Zaffalon, M.; Brofferio, C.; Manna, L.; Beverina, L.; Vedda, A.; Fasoli, M.; Gironi, L.; Brovelli, S. Efficient, fast and reabsorption-free perovskite nanocrystal-based sensitized plastic scintillators. *Nat. Nanotechnol.* **2020**, *15*, 462−468.
8 Yuan, J. W.; Peng, Q. C.; Cao, R. Y.; Yang, Q.; Lei, Y. Y.; Gao, Z. Y.; Wang, Z. Y.; Li, K.; Zang, S. Q. Short lifetime radical metal cluster scintillator. *Angew. Chem. Int. Ed.* **2025**, *64*, e202503457.
9 Luo, A. S.; Zhang, J. R.; Xiao, D. J.; Xie, G. Z.; Xu, X. Q.; Zhao, Q. X.; Sun, C. X.; Li, Y. Z.; Zhang, Z. H.; Li, P.; Luo, S. H.; Xie, X. J.; Peng, Q. M.; Li, H. H.; Chen, R. F.; Chen, Q. S.; Tao, Y.; Huang, W. Efficient metal free organic radical scintillators. *Nat. Commun.* **2024**, *15*, 8181.
10 Chen, X. F.; Song, J. B.; Chen, X. Y.; Yang, H. H. X-ray-activated nanosystems for theranostic applications. *Chem. Soc. Rev.* **2019**, *48*, 3073−3101.
11 Xie, G. Z.; Chen, C.; Zhang, J. R.; Xiao, D. J.; Cai, M. Y.; Gao, Q. Y.; Gao, Z. S.; Sun, C. X.; Li, H.; Li, H. H.; Chen, R. F.; Tao, Y. Evaporation-processed X-ray imaging scintillation screen based on copper clusters. *Chin. J. Org. Chem.* **2025**, *45*, 4219−4226.
12 Chen, Q. S.; Wu, J.; Ou, X. Y.; Huang, B. L.; Almutlaq, J.; Zhumekenov, A. A.; Guan, X. W.; Han, S. Y.; Liang, L. L.; Yi, Z. G.; Li, J.; Xie, X. J.; Wang, Y.; Li, Y.; Fan, D. Y.; Teh, D. B. L.; All, A. H.;

Graphical Abstract

Host-Guest Multiple Resonance Thermally Activated Delayed Fluorescent Copolymer Scintillators for X-ray Imaging

Kai Feng, Zong-Ji Ye, Wei-Guang Wang, Jia-Ni Huang, Xin Yan, Heng-Yu Cao, Zhi-Sheng Gao, Shu-Man Zhang, Si-Ming Chen, Huan-Huan Li, and Ye Tao

Nanjing University of Posts & Telecommunications; Nanjing University

Host-guest multiple resonance thermally activated delayed fluorescent copolymer enables efficient reverse intersystem crossing and high exciton harvesting, yielding intense radioluminescence and flexible X-ray imaging with 13.3 lp/mm resolution and 390 nGy/s detection limit.

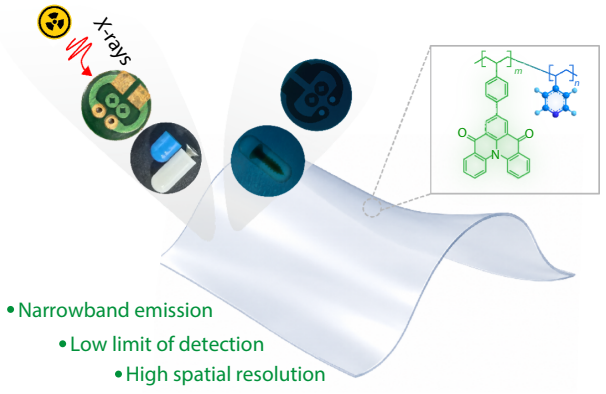

Mohammed, O. F.; Bakr, O. M.; Wu, T.; Bettinelli, M.; Yang, H. H.; Huang, W.; Liu, X. G. All-inorganic perovskite nanocrystal scintillators. *Nature* **2018**, *561*, 88–93.
13 Wang, X.; Shi, H. F.; Ma, H. L.; Ye, W. P.; Song, L. L.; Zan, J.; Yao, X. K.; Ou, X. Y.; Yang, G. H.; Zhao, Z.; Singh, M.; Lin, C. Y.; Wang, H.; Jia, W. Y.; Wang, Q.; Zhi, J. H.; Dong, C. M.; Jiang, X. Y.; Tang, Y. G.; Xie, X. J.; Yang, Y.; Wang, J. P.; Chen, Q. S.; Wang, Y.; Yang, H. H.; Zhang, G. Q.; An, Z. F.; Liu, X. G.; Huang, W. Organic phosphors with bright triplet excitons for efficient X-ray-excited luminescence. *Nat. Photon.* **2021**, *15*, 187–192.
14 Du, X. Y.; Zhao, S.; Wang, L.; Wu, H. D.; Ye, F.; Xue, K. H.; Peng, S. Q.; Xia, J. L.; Sang, Z. R.; Zhang, D. D.; Xiong, Z. P.; Zheng, Z. P.; Xu, L.; Niu, G. D.; Tang, J. Efficient and ultrafast organic scintillators by hot exciton manipulation. *Nat. Photon.* **2024**, *18*, 162–169.
15 Dong, M. Y.; Wang, Z. Y.; Lin, Z. Y.; Zhang, Y. S.; Chen, Z. K.; Wu, Y. M.; Ma, H. L.; An, Z. F.; Gu, L.; Huang, W. Temperature-adaptive organic scintillators for X-ray radiography. *J. Am. Chem. Soc.* **2024**, *147*, 4069–4078.
16 Hou, X. L. Liquid scintillation counting for determination of radionuclides in environmental and nuclear application. *J. Radioanal. Nucl. Chem.* **2018**, *318*, 1597–1628.
17 Chen, M. X.; Sun, L. J.; Ou, X. Y.; Yang, H. H.; Liu, X. G.; Dong, H. L.; Hu, W. P.; Duan, X. F. Organic semiconductor single crystals for X-ray imaging. *Adv. Mater.* **2021**, *33*, 2104749.
18 Dong, C. M.; Wang, X.; Gong, W. Q.; Ma, W. B.; Zhang, M.; Li, J. J.; Zhang, Y.; Zhou, Z. X.; Yang, Z. J.; Qu, S. L.; Wang, Q.; Zhao, Z.; Yang, G. H.; Lv, A. Q.; Ma, H. L.; Chen, Q. S.; Shi, H. F.; Yang, Y.; An, Z. F. Influence of isomerism on radioluminescence of purely organic phosphorescence scintillators. *Angew. Chem. Int. Ed.* **2021**, *60*, 27195–27200.
19 Koshimizu, M. Recent progress of organic scintillators. *Jpn. J. Appl. Phys.* **2023**, *62*, 010503.
20 Ma, W. B.; Su, Y. R.; Zhang, Q. S.; Deng, C.; Pasquali, L.; Zhu, W. J.; Tian, Y.; Ran, P.; Chen, Z.; Yang, G. Y.; Liang, G. J.; Liu, T. Y.; Zhu, H. M.; Huang, P.; Zhong, H. Z.; Wang, K. W.; Peng, S. Q.; Xia, J. L.; Liu, H. F.; Liu, X.; Yang, Y. Thermally activated delayed fluorescence (TADF) organic molecules for efficient X-ray scintillation and imaging. *Nat. Mater.* **2022**, *21*, 210–216.
21 Wang, J. X.; Gutiérrez-Arzaluz, L.; Wang, X. J.; He, T. Y.; Zhang, Y. H.; Eddaoudi, M.; Bakr, O. M.; Mohammed, O. F. Heavy-atom engineering of thermally activated delayed fluorophores for high-performance X-ray imaging scintillators. *Nat. Photon.* **2022**, *16*, 869–875.
22 Wang, X.; Wang, Y. X.; Wang, Y. L.; Liu, H. Z.; Zhang, Y. G.; Liu, W.; Wang, X. X.; Wang, S. Color-tunable X-ray scintillation based on a series of isotypic lanthanide-organic frameworks. *Chem. Commun.* **2020**, *56*, 233–236.
23 Tang, L. L.; Zan, J.; Peng, H.; Yan, X.; Tao, Y.; Tian, D.; Yang, Q. Q.; Li, H. H.; Chen, Q. S.; Huang, W.; Chen, R. F. X-ray excited ultralong room-temperature phosphorescence for organic afterglow scintillators. *Chem. Commun.* **2020**, *56*, 13559–13562.
24 Yang, Z.; Yao, J. S.; Xu, L. M.; Fan, W. X.; Song, J. Z. Designer bright and fast $CsPbBr_3$ perovskite nanocrystal scintillators for high-speed X-ray imaging. *Nat. Commun.* **2024**, *15*, 8870.
25 Gan, N.; Zou, X.; Dong, M. Y.; Wang, Y. Z.; Wang, X.; Lv, A. Q.; Song, Z. C.; Zhang, Y. Y.; Gong, W. Q.; Zhao, Z.; Wang, Z. Y.; Zhou, Z. X.; Ma, H. L.; Liu, X. W.; Chen, Q. S.; Shi, H. F.; Yang, H. H.; Gu, L.; An, Z. F.; Huang, W. Organic phosphorescent scintillation from copolymers by X-ray irradiation. *Nat. Commun.* **2022**, *13*, 3995.
26 Wei, J.; Jiang, Y. Y.; Liu, C. Y.; Duan, J. Y.; Liu, S. Y.; Liu, X. M.; Liu, S. J.; Ma, Y.; Zhao, Q. Organic room-temperature phosphorescent polymers for efficient X-ray scintillation and imaging. *Adv. Photon.* **2022**, *4*, 035002.
27 Tao, Y.; Yuan, K.; Chen, T.; Xu, P.; Li, H. H.; Chen, R. F.; Zheng, C.; Zhang, L.; Huang, W. Thermally activated delayed fluorescence materials towards the breakthrough of organoelectronics. *Adv. Mater.* **2014**, *26*, 7931–7958.
28 Im, Y.; Kim, M.; Cho, Y. J.; Seo, J. A.; Yook, K. S.; Lee, J. Y. Molecular design strategy of organic thermally activated delayed fluorescence emitters. *Chem. Mater.* **2017**, *29*, 1946–1963.
29 Liu, Q.; Chen, W. C.; Zhang, R.; Wei, H. X.; Liu, B.; Jin, J. M.; Liu, Y.; Ye, Z. C.; Chen, J. X.; Ji, S. M.; Zhang, H. L.; Huo, Y. P. Design, synthesis, and electroluminescence of red TADF dyes based on cyanophenanthrene. *Dyes Pigm.* **2023**, *212*, 111125.
30 Arsenyan, P.; Vigante, B.; Leitonas, K.; Volyniuk, D.; Andruleviciene, V.; Skhirtladze, L.; Belyakov, S.; Grazulevicius, J. V. Dual versus normal TADF of pyridines ornamented with multiple donor moieties and their performance in OLEDs. *J. Mater. Chem. C* **2021**, *9*, 3928–3938.
31 Gao, H. L.; Shen, S. G.; Qin, Y. Y.; Liu, G. H.; Gao, T.; Dong, X. Y.; Pang, Z.; Xie, X.; Wang, P. F.; Wang, Y. Ultrapure blue thermally activated delayed fluorescence (TADF) emitters based on rigid sulfur/oxygen-bridged triarylboron acceptor: MR TADF and D-A TADF. *J. Phys. Chem. Lett.* **2022**, *13*, 7561–7567.
32 Yang, Z.; Shi, W. K.; Shao, Z. H.; Xiong, Z. H.; Li, Y. F.; Zhu, M. L.; Wen, W.; Li, C.; Ren, L. B.; Zhao, Z. Y.; Guo, Y. L.; Liu, Y. Q. Elastomer doping strategy for high-efficiency stretchable thermally activated delayed fluorescence polymer organic light-emitting diodes. *Chinese J. Polym. Sci.* **2026**, *44*, 970–979.
33 Li, T. Y.; Zhou, Y. T.; Wang, Z. H.; Tao, F. R.; Wang, L. P.; Li, G. Multicolor-tunable and flexible sodium carboxymethyl cellulose-based ultralong room-temperature phosphorescence materials for advanced information encryption. *Chinese J. Polym. Sci.* **2026**, *44*, 1102–1113.
34 Zhang, Y. W.; Zhang, D. D.; Wei, J. B.; Liu, Z. Y.; Lu, Y.; Duan, L. Multi-resonance induced thermally activated delayed fluorophores for narrowband green OLEDs. *Angew. Chem. Int. Ed.* **2019**, *58*, 16912–16917.
35 Xu, Y. C.; Wang, Q. Y.; Cai, X. L.; Li, C. L.; Wang, Y. Highly Efficient electroluminescence from narrowband green circularly polarized multiple resonance thermally activated delayed fluorescence enantiomers. *Adv. Mater.* **2021**, *33*, 2100652.
36 Luo, X. F.; Ni, H. X.; Ma, H. L.; Qu, Z. Z.; Wang, J.; Zheng, Y. X.; Zuo, J. L. Fused π-extended multiple-resonance Induced thermally activated delayed fluorescence materials for high-efficiency and narrowband OLEDs with low efficiency roll-off. *Adv. Opt. Mater.* **2022**, *10*, 2102513.
37 Shizu, K.; Kaji, H. Comprehensive understanding of multiple resonance thermally activated delayed fluorescence through quantum chemistry calculations. *Commun. Chem.* **2022**, *5*, 53.
38 Liao, C.; Du, M. Q.; Li, C. Photoswitchable spiropyridine enabled photoactuation of polymeric hydrogels under physiological pH conditions. *Chinese J. Polym. Sci.* **2024**, *42*, 1602–1609.
39 Zhao, M. M.; Wan, P.; Shi, J. Q.; Ji, L. Progress in organic material based solid-state X-ray scintillators. *J. Mater. Chem. C* **2025**, *13*, 5424–5438.
40 Xu, Y. K.; Li, Z. H.; Peng, G. Q.; Qiu, F.; Li, Z. Z.; Lei, Y. T.; Deng, Y. J.; Wang, H. X.; Liu, Z. T.; Jin, Z. W. Organic cation design of manganese halide hybrids glass toward low-temperature integrated efficient, scaling, and reproducible X-ray detector. *Adv. Opt. Mater.* **2023**, *11*, 2300216.
41 Ma, M. M.; Wang, J.; Jiang, H.; Chen, Q. S.; Xiao, Y.; Yang, H. H.; Lin, L. Transcranial deep-tissue phototherapy for Alzheimer's disease using low-dose X-ray-activated long-afterglow scintillators. *Acta Biomater* **2023**, *155*, 635–643.
42 Chen, H. M.; Lin, M.; Zhao, C. B.; Zhang, D. W.; Zhang, Y.; Chen, F. H.; Chen, Y.; Fang, X.; Liao, Q.; Meng, H.; Lin, M. J. Highly efficient, low-dose, and ultrafast carbazole X-ray scintillators. *Adv. Opt. Mater.* **2023**, *11*, 2300365.
43 Bliznyuk, V. N.; Seliman, A. F.; Ishchenko, A. A.; Derevyanko, N. A.;

DeVol, T. A. New efficient organic scintillators derived from pyrazoline. *ACS Appl. Mater. Interfaces* **2016**, *8*, 12843–12851.
44 Hua, T.; Cao, X. S.; Miao, J. S.; Yin, X. J.; Chen, Z. X.; Huang, Z. Y.; Yang, C. L. Deep-blue organic light-emitting diodes for ultrahigh-definition displays. *Nat. Photon.* **2024**, *18*, 1161–1169.
45 Huang, T. Y.; Wang, Q.; Zhang, H.; Zhang, Y. W.; Zhan, G.; Zhang, D. D.; Duan, L. Enhancing the efficiency and stability of blue thermally activated delayed fluorescence emitters by perdeuteration. *Nat. Photon.* **2024**, *18*, 516–523.
46 Kamaraj, E.; Kolli, D.; Abburi, R.; Khalid, A.; Hegazy, H. H.; Yahia, I. S.; Ramaraghavulu, R.; Venkatesan, R.; Godumala, M. Purely organic room-temperature phosphorescent materials for OLEDs: molecular design, photophysics, and device strategies. *Dyes Pigm.* **2026**, *249*, 113604.
47 Walia, R.; Xiong, X.; Fan, X. C.; Chen, T. F.; Wang, H.; Wang, K.; Shi, Y. Z.; Tang, X.; Bredas, J. L.; Adachi, C.; Chen, X. K.; Zhang, X. H. Achieving small singlet-triplet energy gaps in polycyclic heteroaromatic emitters. *Nat. Mater.* **2025**, *24*, 1576–1583.
48 Shonde, T. B.; Chaaban, M.; Liu, H.; Olasupo, O. J.; Ben-Akacha, A.; Gonzalez, F. G.; Julevich, K.; Lin, X. S.; Winfred, J.; Stand, L. M.; Zhuravleva, M.; Ma, B. W. Molecular sensitization enabled high performance organic metal halide hybrid scintillator. *Adv. Mater.* **2023**, *35*, 2301612.